Behavior and application of self-centering dampers equipped with buckling-restrained SMA bars

Canxing Qiu [1], Cheng Fang [2,*], Dong Liang [2], Xiuli Du [1], Michael CH Yam [3]

[1] *Key Laboratory of Urban Security and Disaster Engineering of Ministry of Education, Beijing University of Technology, Beijing 100124, China;*

[2] *College of Civil Engineering, Tongji University, Shanghai 200092, China*

[3] *Department of Building & Real Estate, The Hong Kong Polytechnic University, Hung Hom, Kowloon, Hong Kong, China*

** Corresponding author: email: chengfang@tongji.edu.cn, Tel: +86-(0)2165982926*

Abstract: This study proposes a new type of self-centering damper equipped with novel buckling-restrained superelastic shape memory alloy (SMA) bars. The new solution aims to address some critical issues related to degradation and loss of superelasticity observed in existing tension-only SMA-based self-centering devices, and in addition, to encourage enhanced material utilization efficiency. The cyclic tension-compression behavior of individual SMA bars is experimentally studied first, and subsequently, two proof-of-concept self-centering dampers are manufactured and tested. A simple yet effective numerical model capturing the flag-shaped response of the dampers is then established, and a preliminary system-level analysis is finally conducted to demonstrate the effectiveness of the proposed damper in structural seismic control. The individual SMA bar specimens show asymmetrical flag-shaped hysteretic responses with satisfactory self-centering capability and moderate energy dissipation. Through a specially designed configuration, the proposed damper shows desirable symmetrical and stable hysteretic behavior, and maintains excellent self-centering capability at 6% bar strain. The system-level dynamic analysis indicates that the dampers, as a means of retrofitting, could effectively reduce both the peak and residual inter-story drift ratios of a 6-story steel frame. In particular, the mean residual inter-story drift ratio is reduced from over 0.5% to below 0.2% under the maximum considered earthquake (MCE), implying elimination of necessary structural realignment even after strong earthquakes.

Keywords: seismic resilient; self-centering; shape memory alloy (SMA); tension-compression; damper; buckling-restrained; retrofitting.

1. Introduction

Seismic-resilient structures refer to those which exhibit low residual deformation, low damage, and rapid function recoverability after an earthquake. Damping systems are expected to suppress the peak structural dynamic responses and as a result, directly or indirectly reduce the post-earthquake damage. Passive dampers, including fluid viscous, viscoelastic, friction, and metallic-based ones, have been under intensive theoretical development since the 1980s and their wide implementations in building frames started in the 1990s [1]. While these "conventional" dampers can either reduce the peak inter-story drift or maintain a similar peak inter-story drift with a reduced base shear, the residual deformation is not eliminated. It was even found that added damping can sometimes lead to increased residual deformation [2]. Residual deformation is a complementary metric in addition to the commonly used performance indexes such as peak inter-story drift and member ductility. It is a critical index that can more comprehensively characterize the resilience performance of a structure and the potential damage that the system has suffered after an earthquake. A post-earthquake survey suggested that a building is not economically repairable when the residual inter-story drift exceeds 0.5% [3].

The urgent need to establish seismic-resilient communities was reemphasized after the 2011 Christchurch earthquake where hundreds of non-collapsed buildings with significant damages and residual deformations were demolished [4]. Since then, self-centering system has become a very popular research topic in the field of seismic engineering. Self-centering capability in a building structure can be provided by various methods, where post-tensioning (PT) technology is one of them. A typical case is to "upgrade" steel beam-to-column connections with steel PT tendons together with extra energy dissipation components such as mild-steel angles or friction pads [5-8]. Such concept has also been extended to the development of self-centering bracing members [9-13]. However, the

PT technology may have certain limitations including insufficient ductility (especially for braces), complex construction procedure and unwanted large initial internal forces. In the meantime, a unique class of metal called shape memory alloys (SMAs) has been brought into the attention of the researchers. SMAs have two characteristics, namely, superelastic effect (SE) at the austenite phase and shape memory effect (SME) at the martensite phase. Superelastic SMAs are capable of spontaneously recovering a strain of up to 8~10% upon load removal at room temperature, while the residual strain of SMAs with SME has to be recovered via heating [14]. The typical stress-strain curves of SMAs with SE or SME are illustrated in Fig. 1(a).

Superelastic SMAs are more preferred for passive seismic control. The material can be produced into various forms including wires/cables, tendons/bolts, helical springs, Belleville washer springs and ring springs [15-20]. These elements have been used in different structural members such as dampers, beam-to-column connections, braces, and base isolators [21-46]. Regardless of the working principle behind these members, the corresponding SMA elements are typically subjected to cyclic tensile stresses, such that a flag-shaped hysteretic behavior is provided at room temperature. In addition, prestressing is often applied to the SMA elements to improve the recoverability. While many existing experimental and theoretical studies have confirmed the encouraging self-centering performance of the SMA-based members, some practical issues are yet to be solved. For example, functional fatigue (or transformation-induced fatigue) leads to downward movements of the transformation plateaus accompanied by an accumulation of residual strain, a phenomenon which significantly compromises the stiffness, energy dissipation and recoverability of tension-only SMA elements. Fig 1(b) shows the degradation behavior of SMA bars under repeated tension. This issue could be effectively addressed by mobilizing the tension-compression characteristics of SMAs. It has been found that functional fatigue-induced degradation is much less significant when the SMA is under tension-compression reversal loading [47]. This is an inherent property of SMA which is

probably related to the mobility of the crystals during the transition between tension and compression strains.

Another issue is temperature dependency, i.e., the SMA loses SE when the temperature accidentally decreases below the transformation temperature (e.g. Austenite finish temperature A_f, often designed as -10~5 ℃ by material engineers for civil engineering application). In other words, spontaneous self-centering function can be lost for tension-only SMA elements at an unexpectedly low temperature, and as a result the stiffness, strength and energy dissipation of the member rapidly disappear because of the "looseness" of the SMA elements when an earthquake happens. For tension-compression SMA elements, however, they would behave similarly to buckling-restrained braces (BRBs) even when losing superelasticity in extreme weather events (i.e., when the environmental temperature drops below A_f), and is therefore still able to provide stable energy dissipation with no loss of stiffness and strength [48].

In contrast to the vast body of literature available on the tension behavior of superelastic SMAs, the compression response is much less explored. Chen et al. [49] reported that superelastic SMAs in compression can still exhibit flag-shaped stress-strain responses with satisfactory recoverability, but the load resistance is larger than that in tension. Adharapurapu et al. [50] confirmed the asymmetry in tension and compression responses of SMAs in both quasi-static and dynamic loading conditions. Zaki et al. [51] proposed a constitutive model taking account of tension-compression asymmetry of SMAs. Reedlunn et al. [52] used digital image correction technology to provide further details of localized strain of SMAs in compression. More recently, Wang and Zhu [47] enriched the test data pool by examining the cyclic tension-compression behavior of SMA bars with buckling-restrained devices. The potential applications of the bucking-restrained SMA bars were also envisaged, but member- and system-level structural analyses have not yet been carried out.

Building on the existing studies, this paper seeks to develop a novel self-centering damper employing a group of buckling-restrained superelastic SMA bars. The cyclic tension-compression

behavior of individual SMA bars is experimentally studied first, where the influence of cross section geometry is shown. Subsequently, two proof-of-concept self-centering dampers are manufactured and tested. These dampers are designed to behave symmetrically even though the individual SMA bars exhibit asymmetrical hysteretic behavior in tension and compression. A numerical model capturing the key hysteretic response of the dampers is then established, and a preliminary system-level analysis is finally conducted to demonstrate the effectiveness of the proposed damper in structural seismic control.

2. Cyclic behavior of individual SMA bars

2.1 Specimens and test setup

The study commenced with a series of quasi-static cyclic tests on individual buckling-restrained superelastic SMA bars made of commercial Ti-50.8at.%Ni alloy (i.e. 50.8% atomic percentage of nickel with the balance contributed by titanium). The main testing parameter was section geometry, as shown in Table 1. Two types of cross-sections, namely, round section and flat section, were produced for the effective working length of the bars, and the considered loading frequency was 0.0025 Hz. The as-received raw bars, which had a diameter of 12 mm, were first machined to the required shapes at room temperature. To obtain the round section configuration, the raw bar was first threaded at both ends (threaded length = 50 mm) to enable bolted connection. The specimen was then processed with CNC latche machining, leading to a net length of 63 mm and a reduced diameter of 6 mm for the working segment. A transition region with 10 mm radius was prepared to achieve smooth stress transfer and to avoid stress concentration. For the flat SMA bars, wire cutting was conducted directly on the non-reduced bars after the threads were finished. Again, a transition region was reserved to mitigate stress concentration. To minimize possible property variation and deficiency caused by local high temperature during the machining process, coolant was applied for both types of the SMA bars. The specimens were then placed into an electric furnace for annealing. The importance of annealing lies in the precipitation of Ti3Ni4, the existence of which

greatly facilitates the martensitic transformation and hinders plastic flow in the surrounding austenite matrix, and as a result enhances the mechanical properties of the SMA products [14]. Previous studies [19-21] suggested that the appropriate annealing scheme for Ti-50.8at.%Ni could be 400~450 ℃ for 15~30 minutes, depending on the manufacturing process and the size of the specimen. Because of the relatively small size considered for the current SMA bars, an annealing scheme of 400 ℃ for 15 minutes was consistently adopted. Apart from the SMA bars, a buckling-restrained grade Q235 (nominal yield strength = 235 MPa) steel bar was also tested for comparison purpose. The detailed dimensions of the SMA and steel bar specimens are shown in Fig. 2.

The test setup for the individual bars is also shown in Fig. 2. An MTS universal test machine with a load capacity of 250 kN was employed. Load with the predefined loading frequency was applied under displacement control. The test object consisted of the SMA bar specimen, upper and lower holding rods and a detachable buckling-restraining plate (BRP). The two holding rods, which were connected to the SMA bar through threads, were clamped by the hydraulic wedge grips of the universal test machine. The BRP was comprised of a pair of steel plates which were firmly joined via high-strength bolts. The SMA bar specimen passed through the reserved opening of the BRP with a clearance of approximately 1 mm. Such clearance was used to accommodate the Poisson effect when the specimen was in compression. The SMA bars were coated with glassine to reduce the friction. The loading amplitude was controlled by the global strain (i.e., elongation of the bar divided by its working length), starting from ±1% strain and increasing at an interval of 1% strain until ±5% strain. Two identical cycles were applied at each amplitude. The room temperature during the tests varied between 20 and 26 ℃.

2.2 Test results and discussions

Fig. 3 shows the stress-strain responses of the five individual bar specimens. In contrast to the full hysteresis exhibited by the steel bar, the SMA bars show typical flag-shaped hysteretic behavior with much reduced residual strains. It is confirmed that the flag-shaped hysteresis is stable and the

degradation effect is not significant under the considered number of loading cycles. The behavior of the SMA bars varies in the two loading directions, where larger load resistance and "post-yield" hardening stiffness generally occur when subjected to compression. The tension-compression asymmetry is attributed to the crystallographic asymmetry of the martensitic phase transformation. Reedlunn et al. [52] explained this phenomenon using a Gibbs free energy model and a basic thermodynamic theory, and it was found that the product of the "yield" stress (forward transformation stress σ_{Ms}) and the transformation strain (ε_L, see Fig. 1(a)) is similar when in tension and compression. This may explain the larger post-yield hardening stiffness in compression, a case which is related to the smaller ε_L because of the larger σ_{Ms}. In addition, the compressive residual strain is slightly larger than that in tension. After experiencing the maximum considered strain of 5%, a maximum residual strain of around 1% is found in specimen SMA-F-2 in compression, corresponding to a recovery rate (ratio of recovered to maximum strains) of 80%. Less residual strains are observed in the other SMA bar specimens.

Table 2 summarizes the key material properties computed from the stress-strain responses of the SMA bars. The measured Young's modulus ranges from 32.2 to 42.6 GPa, and the value is larger in compression than in tension. For most cases, the "yield" strength in compression is larger than that in tension, with the exception of specimen SMA-F-1. The relatively smaller compressive yield strength for this particular specimen may be attributed to the buckling tendency, noting that there is a clearance within the BRP, and the thin flat cross-section of this specimen is easier to buckle about the weak axis. Once the bar bears against the BRP, further buckling deflection is prevented. From an energy dissipation point of view, the equivalent viscous damping (EVD) can be expressed by:

$$EVD = \frac{W_D}{4\pi W_E} \tag{1}$$

where W_D is the energy dissipation per cycle, i.e., the area of each cycle, and W_E is the energy stored in a linear system undergoing the same maximum displacement. EVD is a dimensionless

measurement of energy dissipation and depends on the shape of the hysteresis [53]. Due to the asymmetry, the EVDs in tension and compression are shown separately, and the total EVD of a complete cycle should be the summation of both. It can be seen that the EVD of a half-cycle ranges between 4.4% and 6.4%, where the variation is clearly attributed to the different shapes of the hysteresis. The geometric configuration does not have a clear influence on the EVD properties.

3. Proposed self-centering dampers

3.1 Working principle of proposed dampers

The asymmetrical hysteretic behavior of individual SMA bars may not be desirable for practical application. Therefore, the main concept of the proposed damper is to enable a symmetrical hysteretic behavior by allowing two groups of SMA bars to work together, where one group is subjected to tension and the other group is concurrently in compression. As typically shown in Fig. 4(a), the proposed damper is comprised of an external frame, an internal frame, two SMA bars (for demonstration purpose only and more bars can be used if necessary), BRPs and other necessary accessories including stiffeners, connecting plates and bolts. For each SMA bar, one end is bolt-connected to the internal frame and the other end is bolt-connected to the external frame. The internal frame can move axially through the slots of the external frame, and such relative movement causes tension force in one bar and compression force in the other. The BRPs, which may be attached to the internal frame or just freely placed, only serve as restrainers and have no contribution to the load resistance.

Fig. 4(b) further illustrates the recommended fabrication steps for the proposed damper. The BRP is first assembled to allow the SMA bar to pass through the reserved opening (step 1). The upper SMA bar is then positioned by fixing its lower end to the upper diaphragm of the internal frame (step 2). At the meantime, the upper end of the SMA bar is connected to a free plate which is part of the external frame (step 3). Subsequently, the lower SMA bar is connected to the bottom

diaphragm of the external frame at one end (step 4). Finally, the external frame is assembled, and the other end of the lower SMA bar is connected to the lower diaphragm of the internal frame (step 5).

3.2 Damper specimens and test arrangement

In order to verify the feasibility of the proposed working principle, two small-scale proof-of-concept damper specimens, namely, D-R and D-F, were produced and tested. The geometric configuration and the detailed dimensions of the two specimens are shown in Fig. 4(a), and they only differed in the type of the SMA bars, i.e., round and flat SMA bars were used for damper specimens D-R and D-F, respectively. The material, dimension and annealing procedure of the round and flat SMA bars used in the dampers are identical to those of the aforementioned individual bars SMA-R-1 and SMA-F-1, respectively. Grade Q345 steel was used for the external and internal frames which always remained elastic. Quasi-static tests with a similar loading frequency to that for the individual bars were performed on the damper specimens. As shown in Fig. 5, the two ends of the damper specimens were directly gripped by the hydraulic wedge grips of the universal test machine. Similar to the individual bar tests, the loading protocol was controlled by the global strain of the SMA bars, where the amplitude started from ±1% strain with an incremental interval of 1% strain until fracture of the SMA bars. Again, two identical loading cycles were performed at each amplitude.

3.3 Test results and discussions

The dampers exhibited anticipated deformation mode during the tests. The internal frame travelled axially in relation to the external frame, which was accompanied by observable elongation or shortening of the SMA bars. Specimen D-F experienced initial bar fracture during the 6% strain cycle, and the same failure mode happened in specimen D-R at 10% bar strain, as shown in Fig. 6. For both cases, the fracture occurred at the very end of the reduced segment near the transition region. Compared with tension only SMA bars where the fracture strain is typically larger than 15%, the reduced ductility of the tension-compression SMA bars was probably due to the local buckling tendency in the unrestrained part which was designed to allow free shortening of the bars [47]. This

may also help explain the earlier fracture of the flat SMA bars in specimen D-F, where local buckling is more likely to happen in the unrestrained "thin plate" segment. Moreover, as the flat SMA bars were machined using wire cutting in contrast to CNC lathe machining for the round bars, the resulting mechanical deficiencies and localized stress concentration may also be responsible for the early fracture. The test phenomenon warned that flat SMA bars should be more cautiously used in the proposed dampers especially when the ductility demand is high. The non-fractured SMA bars were also inspected after the tests. Minor permanent bending deformation was exhibited by the round bar, while for the flat bar, negligible permanent bending was observed. It should be kept in mind that the former had experienced a maximum strain of ±10% whereas the latter had only undergone ±6% strain.

Fig. 7 shows the load-deformation responses of the damper specimens. To enable a clearer observation for specimen D-R, the result up to 6% strain amplitude and the complete test data (until fracture) are shown separately. Except for ductility, the two specimens generally have comparable load-deformation responses because of the same chemical composition and annealing procedure adopted for the flat and round SMA bars. Typical flag-shaped hysteretic responses with satisfactory self-centering capability are observed for both damper specimens. The ascending branch consists of three stages, namely, initial elastic stage, transformation plateau, and martensitic hardening. Importantly, the hysteretic responses are symmetrical in tension and compression, and are quite stable with negligible degradation effect.

Figs. 8(a) through 8(d) show the peak load, residual deformation, energy dissipation per complete cycle, and EVD of the damper specimens as a function of deformation. As each cycle involves one SMA bar in tension and one in compression, i.e., the response is generally symmetrical, the average values obtained from the positive and negative loading directions were given for quantities like peak load and residual deformation. The peak load, as shown in Fig. 8(a), increases with increasing deformations, indicating pronounced cyclic hardening. For specimen D-R, the

increase of the peak load becomes more remarkable beyond 6% bar strain, which is due to the martensitic hardening of the SMA. As shown in Fig. 8(b), very limited residual deformation is induced prior to 6% bar strain, corresponding to a recovery rate of more than 90%. The residual deformation is more rapidly accumulated afterwards (for specimen D-R). The damper specimens show moderate energy dissipation capabilities. The energy dissipation per cycle increases with an increase in deformation because of the growing hysteresis (Fig. 8(c)). As seen in Fig. 8(d), the maximum EVD is 11.5% which occurs at 6% bar strain. The EVD slightly decreases afterwards, which could be attributed to the more remarkable increase in the peak load and as a result a significant increase in W_E (see Eq. (1)). The above responses suggest that in order to achieve satisfactory self-centering and energy dissipation capabilities and a remote risk of fracture, 6% bar strain seems to be a reasonable design-based limit for practical use of buckling-restrained SMA bars. This limit may be relaxed for round SMA bars which have better ductility than flat bars. The design considerations are discussed in more detail in the next section.

4. Numerical investigations

4.1 Modelling of damper and validation

Following the experimental study, a numerical investigation is conducted to evaluate the effectiveness of the proposed damper in seismic control. To simulate the cyclic behaviour of the damper, a simple yet effective numerical model is developed in the nonlinear finite element program OpenSees [54]. As can be seen from the test results, the hysteresis "width" of the damper is getting larger as the loading amplitude increases, and residual deformation is induced at late loading stages. To reasonably capture this feature, the damper is represented by a parallel combination of two truss elements, which are designated with the material models *Steel02* and *SelfCentering*, respectively, as illustrated in Fig. 9(a). In other words, the cyclic behaviour of the damper can be considered as a superposition of a flag-shaped self-centring damper and a steel damper. The *Steel02* material is used to better capture the smooth stress transition during cyclic loading. The corresponding parameters R0,

cR1, cR2, a1, a2, a3, and a4 are set to be 18, 0.925, 1, 0, 1, 0, 1, and 0, respectively (details of these parameters are given in the OpenSees manual [54]). The two truss elements are coupled in terms of their deformations. Being consistent with the loading condition considered in the experiments, displacement-based cyclic loading loops are applied to the numerical model, and Newton's solution algorithm is used to solve the nonlinear algebraic equations. Through proper tuning of the material properties, the model can be conveniently calibrated to reflect the actual test results. Fig. 9(b) compares the simulation outcome together with the experimental data for damper specimen D-R, where a good agreement is shown. The main input parameters for the damper model are given in Table 3. The total cross-sectional area, A, and the length, L, of the elements are same as that of the tested damper. The "yield" strength σ_y is taken as 400 MPa, which is approximately the average value of tension and compression responses. The elastic modulus E is slightly lower than the experimental value in order to consider other possible sources of deformation (e.g., deformation of the steel frames) in the damper. The values of α, β, ε_{bear} and γ are estimated according to the test results. The simulation technique developed for the proposed dampers is deemed feasible and is therefore consistently used in the subsequent system-level analyses.

4.2 Design and modelling of prototype buildings

The 6-story frame originally designed for FEMA P-751 [55] is selected to demonstrate the effectiveness of the proposed damper in reducing seismic demands. The frame is located at a Class C site in Seattle, Washington. As reported by prior studies [55−56], the frame is relatively weak at the bottom stories, and dampers are thus suggested to enhance the seismic performance. Fig. 10(a) shows the plain layout and elevation view of the original frame. There are a total of 10 lateral load resisting bays in the entire frame in the considered SN seismic input direction, and half of them are chosen for analysis due to symmetry. The 2D frame for the analysis has a constant bay width of 8.53 m, and the story height is 4.57 m for the 1st story and 3.81 m for the upper stories. The seismic

masses are 1.248×10^6, 1.237×10^6, and 1.242×10^6 kg for the first, roof, and other levels, respectively. Additional structural details can be found in the literature [55−56].

For comparison purpose, a retrofitted version of the frame, employing diagonally placed self-centering dampers, is designed, as shown in Fig. 10(b). For this emerging damper, the corresponding seismic design methodology is not available in the current codes or seldom reported by the relevant studies. In addition, the hysteretic characteristics and possible residual deformation of the proposed SMA damper cannot be explicitly considered by the design methods that have been developed for existing SMA dampers [57−59]. In light of these, three basic design rules are provisionally defined in the present study: 1) the dampers are sized according to the designed-basis earthquake (DBE) spectrum; 2) the effective length of the SMA bars is determined in such a way that when the retrofitted frame is designed with a target inter-story drift of around 2.0%, the corresponding strain sustained by the SMA bars reaches 6%, a strain level which ensures reliable recoverability; and 3) for the residual deformation response, the controlled system needs to meet at least the DS1 and DS2 classes stipulated in FEMA P-58 [60], at the DBE and maximum considered earthquake (MCE) levels, respectively. Class DS1 requires that the maximum residual inter-story drift ratio of a building does not exceed 0.2% such that "no structural realignment is necessary for structural stability, but the building may require adjustment and repairs to non-structural and mechanical components" [60]. Class DS2 defines a relaxed residual inter-story drift ratio limit of 0.5% such that post-earthquake repair work is economically feasible, and structural stability is minimally compromised. Classes DS3 and DS4 are associated with increased residual inter-story drift ratio limits which either jeopardize repairability or put the structure in danger of collapse during aftershocks. Based on the above rules and considering the inverted V-bracing configuration, the SMA dampers are designed accordingly, with the basic mechanical properties given in Table 4. It can be easily calculated from the table that a total number of 48 SMA bars (4 bars per damper × 12 dampers) are used for the considered 2D retrofitted frame. It should be noted that a V-bracing configuration would result in symmetrical floor

response even if the two adjacent braces behave differently, so only one group of SMA bars can be alternatively used for each brace, which makes the core device shorter/more compact. For single diagonal braces, the SMA bars have to be placed in pairs in the device (one group in tension and the other group in compression).

The finite element models of the original and retrofitted braced frames are built in OpenSees [54]. Focusing on the 2D frame, the associated seismic tributary mass is half of the total floor mass. A leaning column that carries the necessary seismic mass is coupled with the frame at each floor level in order to reflect the P-Δ effect. The leaning columns are placed vertically next to the 2D frame, and the nodes of the leaning columns are connected to the corresponding edge nodes of the frame through rigid links. All the nodes in the leaning columns and rigid links are pin-connected. The main boundary members are modelled with force-based beam–column elements, and the dampers are modelled with the aforementioned simulation technique. The yield strength of the structural steel is assumed to be 375 MPa. The obtained fundamental periods of vibration for the uncontrolled and controlled structures are 2.02 and 1.61 s, respectively, and the static pushover responses are compared in Fig. 11. For the uncontrolled frame, a negative tangent stiffness starts at 2.51%, which agrees well with the independent study reported in [55]. Conversely, the controlled frame exhibits positive tangent stiffness, thanks to the increased load carrying capacity enabled by the extra dampers.

4.3 Ground motions

The seismic performance of the uncontrolled and controlled frames under both the DBE and MCE hazard levels are evaluated. The original prototype frame was designed using the design spectrum with the spectral acceleration parameters of S_{DS} = 1.09 g, S_{D1} = 0.494 g and the long-period transition period T_L = 6 s [61]. To realistically simulate the essential characteristics of the ground motions in Seattle, the SAC ground motion records developed for the city are utilized. The 20 DBE records (designated as SE01-SE20) with a probability of exceedance of 10% in 50 years were

adopted. Being in accordance with the scaling procedure conducted by the original report [55], the ground motion records were re-scaled such that no ordinate of the mean response spectrum falls below the design spectrum over the period range from 0.2T to 1.5T, where T is the fundamental period of vibration of the prototype frame. The re-scaled ground motions are further scaled up to the MCE level by multiplying the accelerogram by 1.5. The maximum duration of each ground motion record is extended by adding zero accelerations for 30 seconds, which allows the structural vibration to completely decay.

Fig. 12 shows the individual and mean elastic response spectra of the selected ground motions for the 5% damped single-degree-of-freedom (SDOF) systems. The mean response reasonably matches the target spectrum over the interested period range on the conservative side. Substantial record-to-record variability can be clearly noticed among the considered ground motion suite and therefore the mean seismic response is of particular interest in the seismic performance evaluation.

4.4 Structural responses and discussions

Fig. 13(a) plots the mean height-wise peak and residual inter-story drift ratios as well as the peak floor accelerations of the uncontrolled and controlled frames under the DBE. The results indicate that the peak inter-story drift ratio of the controlled frame is effectively reduced in the lower three stories in comparison against the uncontrolled frame. Specifically, the mean maximum inter-story drift ratio after using the SMA dampers is decreased from 1.90% to 1.67%, corresponding to an approximately 12% reduction. The mean inter-story drift ratio is larger than 1.5%, which means that the nonlinearity of the dampers have been well mobilized. It is believed that the reduction in the peak inter-story drift ratio response is jointly attributed to the added stiffness and damping provided by the SMA dampers. Regarding the residual inter-story drift ratio, the mean response of the uncontrolled frame violates the DS1 requirement, whereas the controlled frame has a sufficient safety margin from this limit. The mean maximum residual inter-story drift ratio among all the floors is decreased by approximately 40% after using the SMA dampers. This suggests that the SMA dampers are more

efficient in reducing the residual inter-story drift ratio than reducing the peak one under the DBE. It is also found in Fig. 13(a) that the peak floor accelerations are nearly unaffected by the dampers, although the controlled frame is "stiffened".

The mean responses of the frames under the MCE are further shown in Fig. 13(b). It is clearly seen that both the peak and residual inter-story drift ratios are amplified under the intensified seismic excitations. The mean maximum inter-story drift ratio of the uncontrolled frame is approximately 3.15%, and the presence of the SMA dampers reduces this demand by approximately 17%. The story-wise nonuniform response also becomes less significant after the proposed dampers are installed. From the self-centering capability point of view, the uncontrolled frame suffered from over 0.5% residual inter-story drift ratios on average at the lower three stories, which violates the DS2 limit. As mentioned, this level of residual deformation implies that the post-event repair would be technically challengeable and economically unfeasible [3, 55]. For the controlled frame, the mean maximum residual inter-story drift ratio is dramatically decreased by 70% to less than 0.2%, which meets the DS1 requirement. Being consistent with the observation from the DBE analysis, the peak floor accelerations are not evidently affected at the MCE level. It is worth noting that the strain of the SMA bar could be large under some ground motion records. While the currently adopted model does not account for the occurrence of material failure, the general behavior of the system and the effectiveness of the SMA-based dampers could still be adequately captured, albeit somewhat idealized.

A representative case under the ground motion SE01 × 1.5 is selected to show the typical behavior of the frames. Fig. 14(a) compares the time-history responses of the roof drift ratio between the uncontrolled and controlled frames. It is clear to see that the SMA dampers well reduce both the peak and residual deformations of the system. In this particular case, the peak roof drift ratio is decreased from 4.35% to 2.38% and the residual roof drift ratio is significantly reduced from over 1.3% to nearly zero. Fig. 14(b) gives a close look at the local performance of the controlled frame by

plotting the typical force-deformation histories of the 4th-story braces. As shown in the figure, the final residual deformation under dynamic shakedown is reasonably small, although the damper has well advanced into the nonlinear stage. The individual damper response echoes the minimal residual inter-story drift ratio of the system, and clearly, the excellent self-centering capability provided by the SMA bars in both tension and compression plays a critical role.

5. Summary and conclusions

This paper presents a novel self-centering damper adopting buckling-restrained superelastic SMA bars. The design concept was first validated by a series of cyclic loading tests on individual buckling-restrained SMA bars. In the later proof-of-concept damper test, a pair of SMA bars were utilized for each damper, where at any loading direction, one bar was in tension and the other one was in compression. The cross-sectional shape of the SMA bars was the main testing parameter for the damper specimens. Following the experimental work, the seismic performance of a retrofitted building frame equipped with the proposed dampers was evaluated and compared with the uncontrolled original prototype frame through numerical analysis. Both the DBE and MCE hazard levels were considered, and the main conclusions are summarized as follows:

- The individual SMA bar specimens with an appropriate annealing procedure showed stable flag-shaped hysteretic responses with satisfactory self-centering capability and moderate energy dissipation.
- Although one single SMA bar had obvious asymmetrical tension-compression behavior, the proposed damper generally showed more desirable symmetrical behavior through the proposed configuration. In addition, the cyclic behavior was quite stable with negligible degradation effect.
- The damper maintained excellent self-centering capability of up to 6% bar strain, and the associated equivalent viscous damping ratio was 11.5%. The SMA bars fractured near the transition region at a strain of up to 10%, and such failure mode limited the overall ductility of the damper.

- The SMA bars machined with either round or flat reduced section type enabled the damper to exhibit symmetrical and stable self-centering behavior, but the flat section bars which exhibited a reduced fracture strain should be more cautiously used in practice.
- A simple yet effective numerical simulation technique was proposed for the damper, and a good agreement was found between the simulation result and the experimental data.
- The system-level dynamic analysis confirmed that the damper could effectively reduce the peak and residual inter-story drift ratios. Specifically, the reduction of the peak inter-story drift ratio is over 15%, and that of the residual inter-story drift ratio can achieve 70%. In particular, at the MCE level, the mean residual inter-story drift ratio is reduced from over 0.5% to below 0.2%, implying elimination of necessary structural realignment even after strong earthquakes. The installation of the dampers had little effect on the peak floor acceleration of the system.

Acknowledgement

This research was supported by the National Natural Science Foundation of China (No.: 51808317 and 51778456) and Beijing Postdoctoral Research Foundation, China (Grant No. ZZ2019-104). However, any opinions, findings, conclusions and recommendations presented in this paper are those of the authors and do not necessarily reflect the views of the sponsors. Finally yet importantly, the authors wish to thank the anonymous reviewers for their careful evaluations and insightful comments that helped improve the paper.

References

[1] Castaldo P. Integrated seismic design of structure and control systems. New York: Springer International Publishing, 2014.

[2]Karavasilis TL, Seo CY. Seismic structural and non-structural performance evaluation of highly damped self-centering and conventional systems. Engineering Structures 2011;33:2248–2258.

[3] McCormick J, Aburano H, Ikenaga M, Nakashima M. Permissible residual deformation levels for building structures considering both safety and human elements. Proc. 14th World Conf. Earthquake Engineering, Seismological Press of China, Beijing, 2008.

[4] Wood A, Noy I, Parker M. The Canterbury rebuild five years on from the Christchurch earthquake. Reserve Bank of New Zealand Bulletin 2016;79(3):1–16.

[5] Christopoulos C, Filiatrault A, Uang CM, Folz B. Posttensioned energy dissipating connections for moment-resisting steel frames. Journal of Structural Engineering 2002;128(9):1111-20.

[6] Li Z, He M, Wang K. Hysteretic performance of self-centering glulam beam-to-column connections. Journal of Structural Engineering 2018;144(5):04018031.

[7] Zhang AL, Zhang YX, Li R, Wang ZY. Cyclic behavior of a prefabricated self-centering beam–column connection with a bolted web friction device. Engineering Structures 2016;111: 185-198.

[8] Lin YC, Sause R, Ricles JM. Seismic performance of a steel self-centering moment resisting frame: hybrid simulations under design basis earthquake. Journal of Structural Engineering ASCE 2013; 139(11): 1823-1832.

[9] Chou CC, Chen YC. Development of steel dual-core self-centering braces: quasi-static cyclic tests and finite element analyses. Earthquake Spectra 2015;31(1):247-272.

[10] Chou CC, Chen YC, Pham DH, Truong VM. Steel braced frames with dual-core SCBs and sandwiched BRBs: mechanics, modeling and seismic demands. Eng Struct 2014;72:26-40.

[11] Chou CC, Wu TH, Beato ARO, Chung PT, Chen YC. Seismic design and tests of a full-scale one-story one-bay steel frame with a dual-core self-centering brace. Engineering Structures 2016;111:435-50.

[12] Erochko J, Christopoulos C, Tremblay R. Design and testing of an enhanced-elongation telescoping self-centering energy-dissipative brace. J. Struct. Eng. 2015;141(6):04014163.

[13] Wang W, Fang C, Zhao Y, Sause R, Hu S, Ricles J. Self-centering friction spring dampers for seismic resilience. Earthquake Engineering & Structural Dynamics 2019;48(9):1045-1065.

[14] Fang C, Wang W. (2019). Shape memory alloys for seismic resilience. Springer. DOI: 10.1007/978-981-13-7040-3

[15] Fang C, Zheng Y, Chen J, Yam MCH, Wang W. Superelastic NiTi SMA cables: Thermal-mechanical behavior, hysteretic modelling and seismic application. Engineering Structures 2019;183: 533-549.

[16] Fang C, Yam MCH, Ma HW, Chung KF. Tests on superelastic Ni–Ti SMA bars under cyclic tension and direct-shear: towards practical recentring connections. Materials and Structures 2015;48(4):1013-30.

[17] Fang C, Zhou XY, Osofero AI, Shu Z, Corradi M. Superelastic SMA Belleville washers for seismic resisting applications: experimental study and modelling strategy. Smart Materials and Structures 2016;25:105013.

[18] Fang C, Yam MCH, Lam ACC, Zhang YY. Feasibility study of shape memory alloy ring spring systems for self-centring seismic resisting devices. Smart Materials and Structures 2015;24:075024.

[19] Wang W, Fang C, Liu J. Large size superelastic SMA bars: heat treatment strategy, mechanical property and seismic application. Smart Materials and Structures 2016;25(7):075001.

[20] Wang W, Fang C, Yang X, Chen YY, Ricles J, Sause R. Innovative use of a shape memory alloy ring spring system for self-centering connections. Engineering Structures 2017;153:503–515.

[21] Wang W, Fang C, Zhang A, Liu X. Manufacturing and performance of a novel self-centring damper with shape memory alloy ring springs for seismic resilience. Struct Control Health Monit 2019; e2337.

[22] Fang C, Wang W, Zhang A, Sause R, Ricles J, Chen Y. Behavior and design of self-centering energy dissipative devices equipped with superelastic SMA ring springs. Journal of Structural Engineering, In press.

[23] Parulekar YM, Ravi Kiran A, Reddy GR, Singh RK, Vaze KK. Shake table tests and analytical simulations of a steel structure with shape memory alloy dampers. Smart Materials & Structures 2014; 23(12):125002.

[24] Dieng L, Helbert G, Chirani SA, Lecompte T, Pilvin P. Use of Shape Memory Alloys damper device to mitigate vibration amplitudes of bridge cables. Engineering Structures 2013; 56: 1547-1556.

[25] Torra V, Auguet C, Isalgue A, Carreras G, Terriault P, Lovey FC. Built in dampers for stayed cables in bridges via SMA. The SMARTeR-ESF project: a mesoscopic and macroscopic experimental analysis with numerical simulations. Engineering Structures 2013; 49: 43-57.

[26] Speicher MS, Desroches R, Leon RT. Experimental results of a NiTi shape memory alloy (SMA)-based recentering beam-column connection. Engineering Structures 2011; 33(9):2448-2457.

[27] Fang C, Yam MCH, Lam ACC, Xie LK. Cyclic performance of extended end-plate connections equipped with shape memory alloy bolts. Journal of Constructional Steel Research 2014;94(94):122-136.

[28] Yam MCH, Fang C, Lam ACC, Zhang YY. Numerical study and practical design of beam-to-column connections with shape memory alloys. Journal of Constructional Steel Research 2015;104:177-192.

[29] Wang W, Fang C, Liu J. Self-centering beam-to-column connections with combined superelastic SMA bolts and steel angles. Journal of Structural Engineering 2017;143(2):04016175.

[30] Fang C, Wang W, He C, Chen YY. Self-centring behaviour of steel and steel-concrete composite connections equipped with NiTi SMA bolts. Engineering Structures 2017;150:390-408.

[31] Fang C, Wang W, Ricles J, Yang X, Zhong Q, Sause R, Chen Y. Application of an innovative SMA ring spring system for self-centering steel frames subject to seismic conditions. Journal of Structural Engineering 2018,144(8):04018114.

[32] Fang C, Yam MCH, Chan TM, Wang W, Yang X, Lin X. A study of hybrid self-centring connections equipped with shape memory alloy washers and bolts. Engineering Structures 2018;164: 155-168.

[33] Qiu C, Zhu S. Shake table test and numerical study of self-centering steel frame with SMA braces. Earthquake Engineering & Structural Dynamic 2017; 46(1):117–137.

[34] Zhu S, Qiu CX. Incremental dynamic analysis of highway bridges with novel shape memory alloy isolators. Advances in Structural Engineering 2014;17(3):429-38.

[35] Bhuiyan AR, Alam MS. Seismic performance assessment of highway bridges equipped with superelastic shape memory alloy-based laminated rubber isolation bearing. Engineering Structures 2013;49:396–407.

[36] Ozbulut OE, Hurlebaus S. Seismic assessment of bridge structures isolated by a shape memory alloy/rubber-based isolation system. Smart Materials & Structures 2010; 20(1): 015003.

[37] Qian H, Li H, Song G. Experimental investigations of building structure with a superelastic shape memory alloy friction damper subject to seismic loads. Smart Materials & Structures 2016; 25: 125026

[38] Seo J, Rogers LP, Hu JW. Computational seismic evaluation of a curved prestressed concrete I-girder bridge equipped with shape memory alloy. European Journal of Environmental and Civil Engineering 2018, In press.

[39] Gao N, Jeon JS, Hodgson DE, DesRoches R. An innovative seismic bracing system based on a superelastic shape memory alloy ring. Smart Materials & Structures 2016; 25: 055030.

[40] Wang B, Zhu S. Superelastic SMA U-shaped dampers with self-centering functions. Smart Materials & Structures 2018; 27: 055003.

[41] Zheng Y, Dong Y, Li Y. Resilience and life-cycle performance of smart bridges with shape memory alloy (SMA)-cable-based bearings. Construction and Building Materials 2018; 158: 389-400.

[42] Miller DJ, Fahnestock LA, Eatherton MR. Development and experimental validation of a nickel–titanium shape memory alloy self-centering buckling-restrained brace. Engineering Structures 2012, 40: 288-298.

[43] Xu X, Zhang Y, Luo Y. Self-centering eccentrically braced frames using shape memory alloy bolts and post-tensioned tendons. Journal of Constructional Steel Research 2016; 125: 190-204.

[44] Seo J, Kim Y, Hu J. Pilot study for investigating the cyclic behavior of slit damper systems with recentering shape memory alloy (SMA) bending bars used for seismic restrainers. Applied Sciences 2015; 5(3): 187-208.

[45] Seo J, Hu J. Seismic response and performance evaluation of self-centering LRB isolators installed on the CBF building under NF ground motions. Sustainability 2016; 8(2): 109.

[46] Seo J, Hu J, Kim KH. Analytical investigation of the cyclic behavior of smart recentering T-Stub components with superelastic SMA bolts. Metals 2017, 7(10): 386.

[47] Wang B, Zhu S. Cyclic tension–compression behavior of superelastic shape memory alloy bars with buckling-restrained devices. Construction and Building Materials 2018;186:103-113.

[48] Liu Y, Xie Z, Van Humbeeck J, Delaey L. Asymmetry of stress–strain curves under tension and compression for NiTi shape memory alloys. Acta Materialia 1998;46(12):4325-4338.

[49] Chen WW, Wu Q, Kang JH, Winfree NA. Compressive superelastic behavior of a NiTi shape memory alloy at strain rates of 0.001–750 s^{-1}. International Journal of Solids and Structures 2001;38(50-51):8989-8998.

[50] Adharapurapu RR, Jiang F, Vecchio KS, Gray III GT. Response of NiTi shape memory alloy at high strain rate: A systematic investigation of temperature effects on tension–compression asymmetry. Acta materialia 2006;54(17):4609-4620.

[51] Zaki W, Moumni Z, Morin C. Modeling tensile-compressive asymmetry for superelastic shape memory alloys. Mechanics of Advanced Materials and Structures 2011;18(7):559-564.

[52] Reedlunn B, Churchill CB, Nelson EE, Shaw JA, Daly SH. Tension, compression, and bending of superelastic shape memory alloy tubes. Journal of the Mechanics and Physics of Solids 2014;63:506-537.

[53] Chopra AK. Dynamics of structures. In: Theory and applications to earthquake engineering. 4th ed. Prentice Hall; 2012.

[54] OpenSees. 2013. Open system for earthquake engineering simulation (OpenSees), v 2.4.1 [Computer software]. Pacific Earthquake Engineering Research Center, Berkeley, CA.

[55] FEMA. 2012. 2009 NEHRP recommended seismic provisions: design examples. FEMA P-751, Washington, DC: FEMA.

[56] Silwal B, Michael RJ, Ozbulut OE. A superelastic viscous damper for enhanced seismic performance of steel moment frames. Engineering Structures 2015;105:152-164.

[57] Qiu C, Zhu S. Performance-based seismic design of self-centering steel frames with SMA-based braces. Engineering Structures 2017;130:67-82.

[58] Qiu C, Li H, Ji K, Hou H, Tian L. Performance-based plastic design approach for multi-story self-centering concentrically braced frames using SMA braces. Engineering Structures 2017;153:628-638.

[59] Qiu C, Qi J, Chen C. Energy-based seismic design methodology of SMABFs using hysteretic energy spectrum. Journal of Structural Engineering (2019), In press.

[60] FEMA. 2012. Seismic performance assessment of buildings. Vol. 1: Methodology. FEMA P-58-1. Washington, DC: FEMA.

[61] Somerville PG, Smith N, Punyamurthula S, Sun J. Development of ground motion time histories for phase 2 of the FEMA/SAC steel project. SAC/BD-97/04, SAC Joint Venture, Sacramento, CA, 1997.

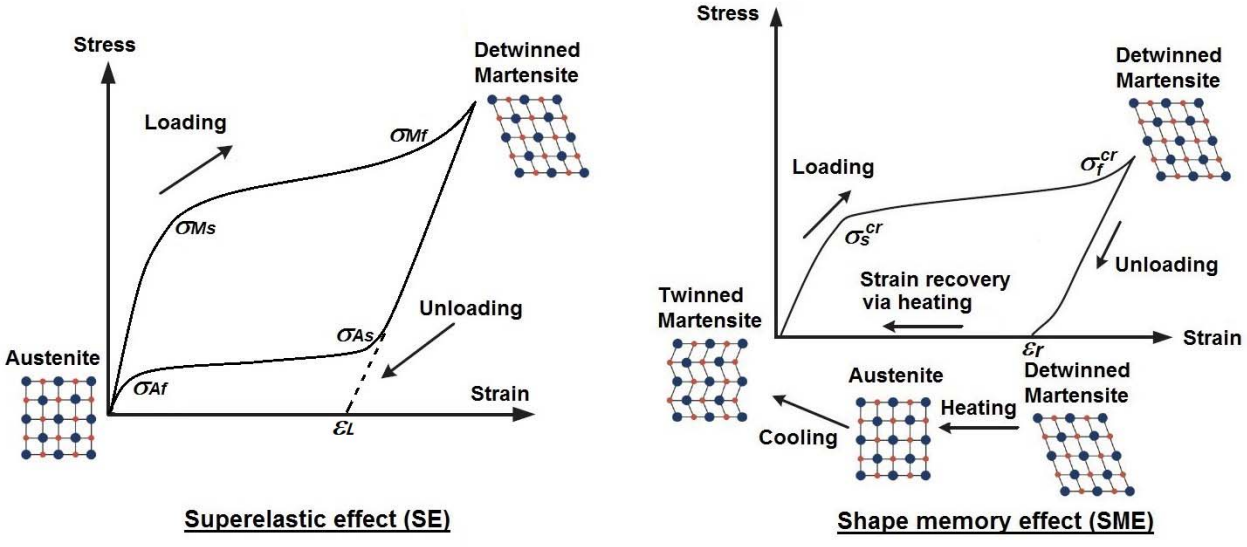

(a)

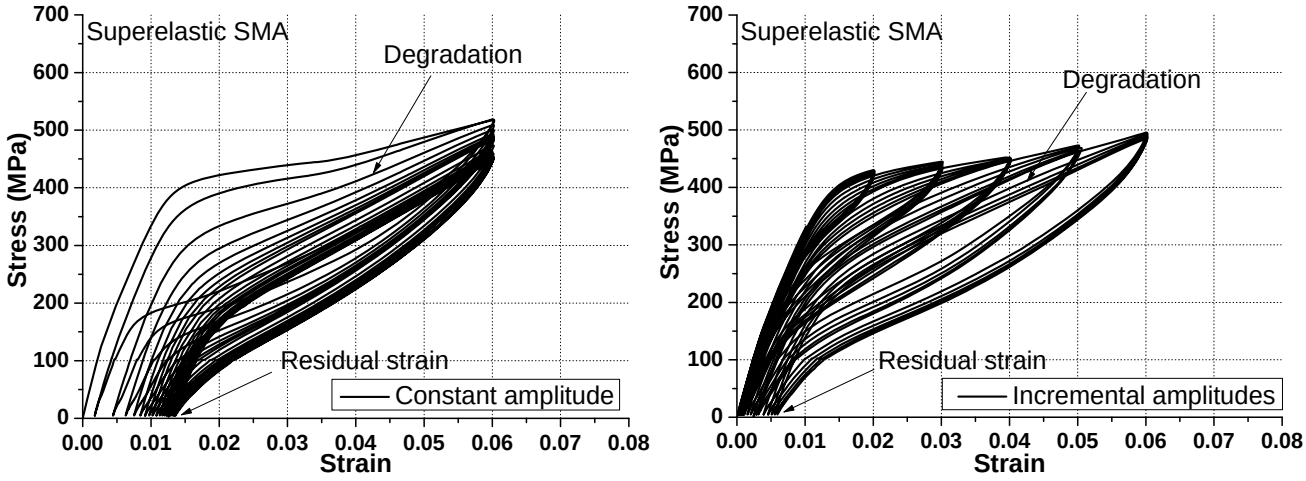

(b)

Fig. 1 Basic material properties of SMA: a) illustration of SE and SME, b) typical stress-strain relationships of superelastic SMA

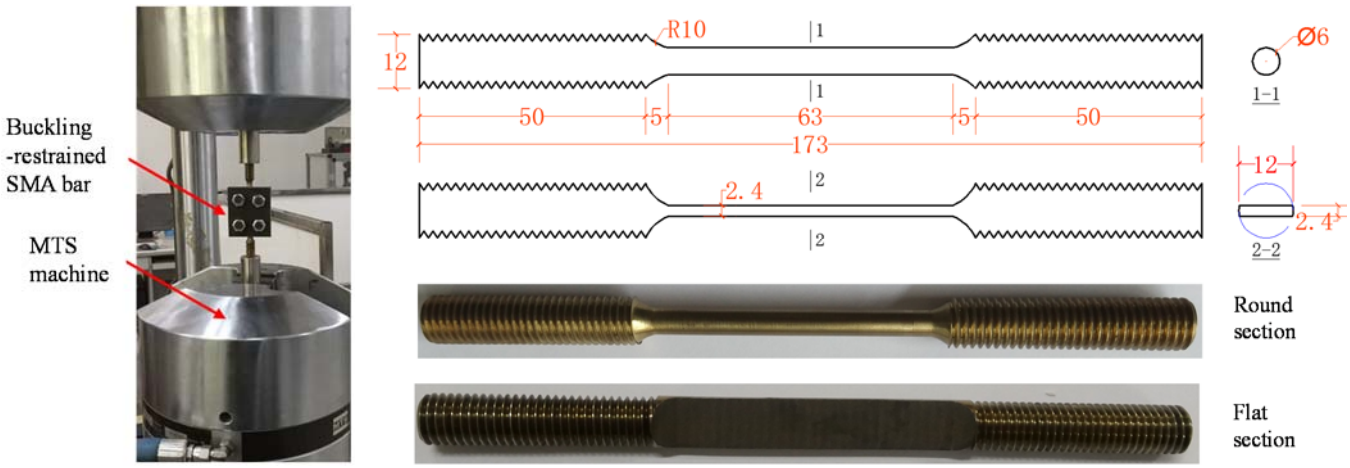

Fig. 2: Typical test setup and details of machined SMA bar specimens

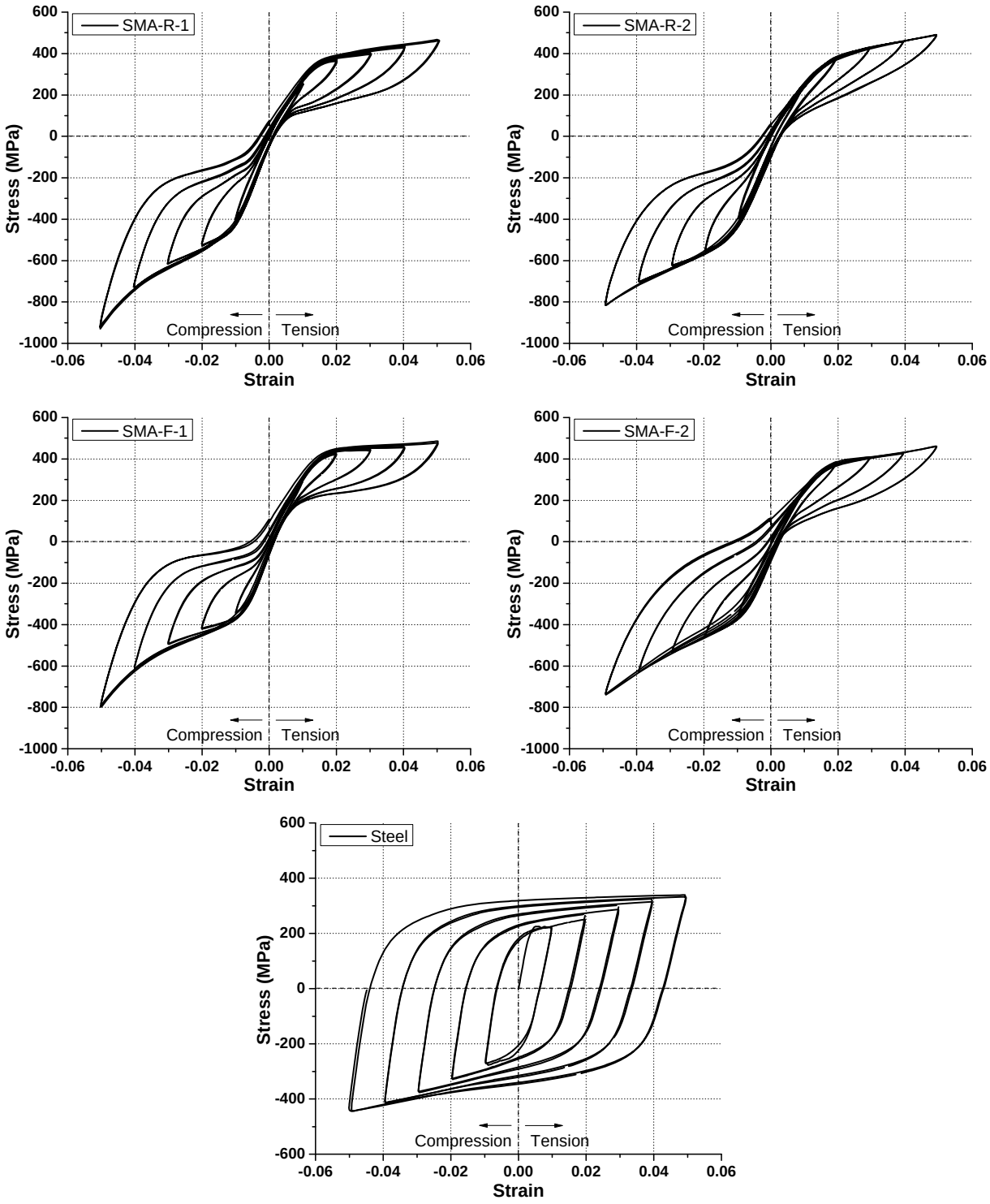

Fig. 3 Stress-strain responses of individual buckling-restrained bar specimens

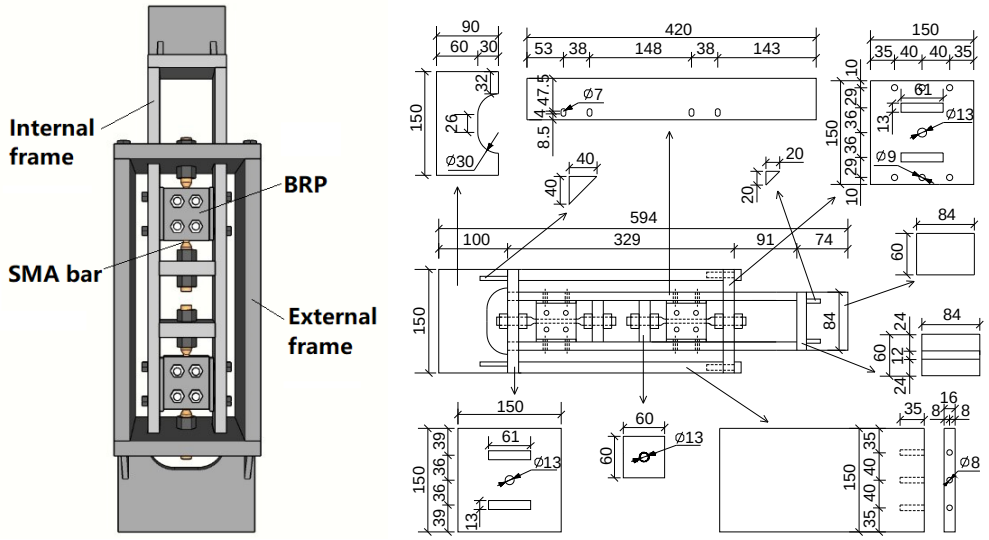

(a)

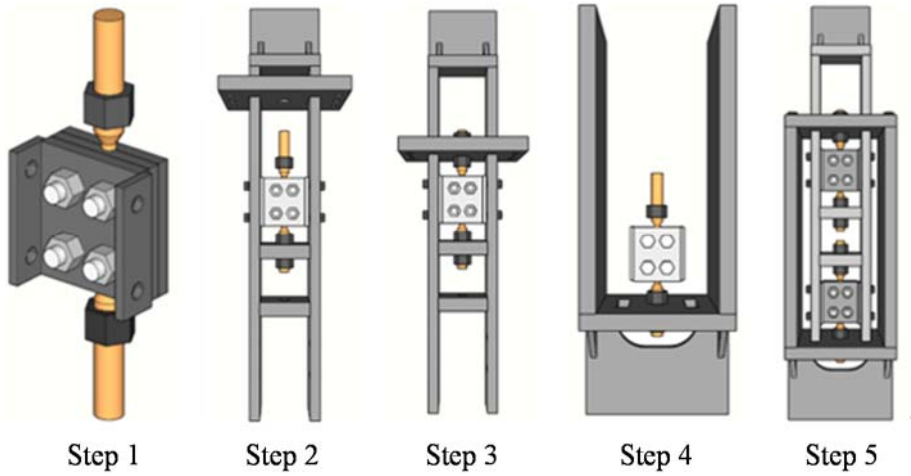

(b)

Fig. 4 Proposed self-centering dampers: a) overall configurations and dimensions, b) typical fabrication steps

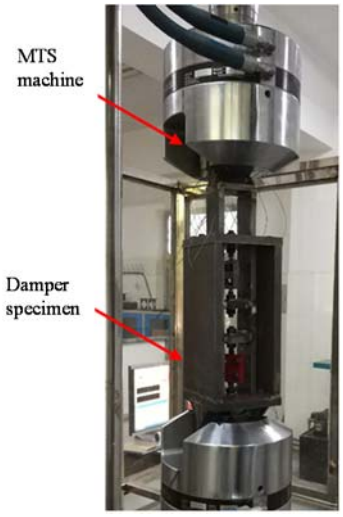

Fig. 5 Test arrangement for proposed damper specimens

Fig. 6 Failure response of SMA bars

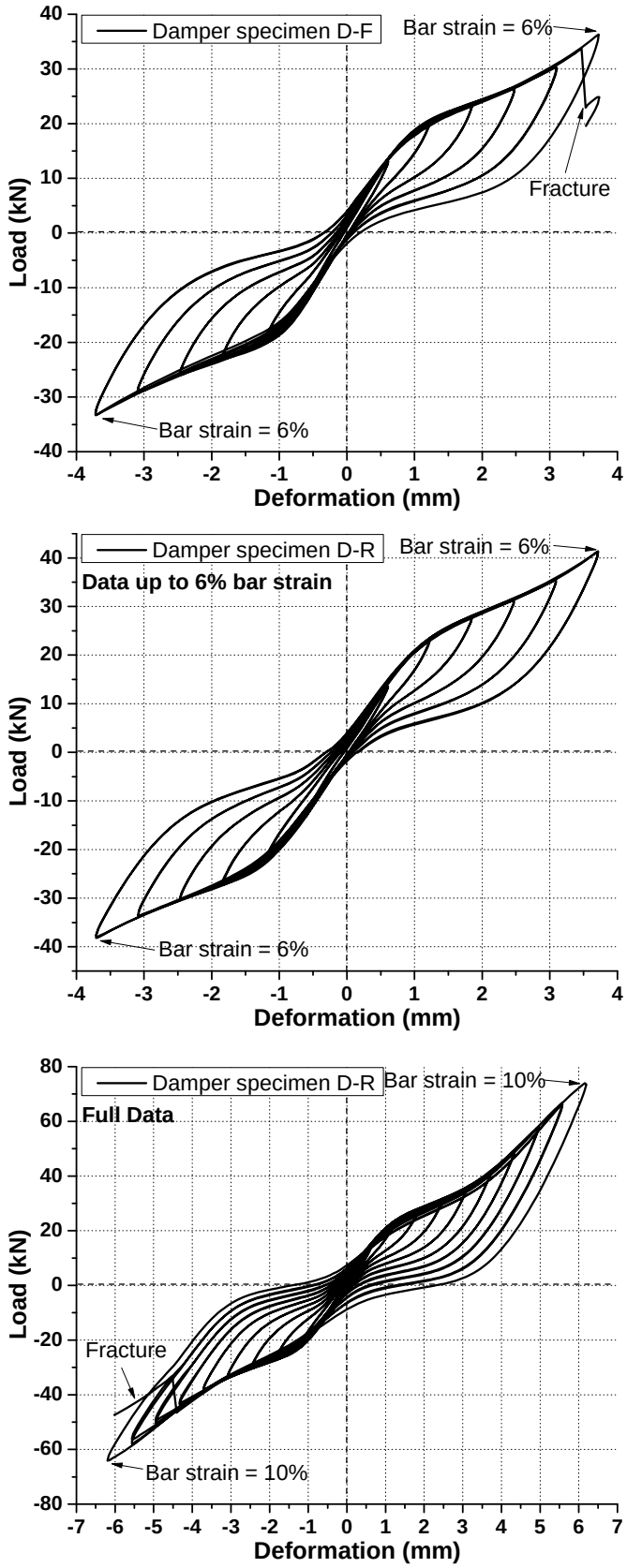

Fig. 7 Load-deformation responses of damper specimens

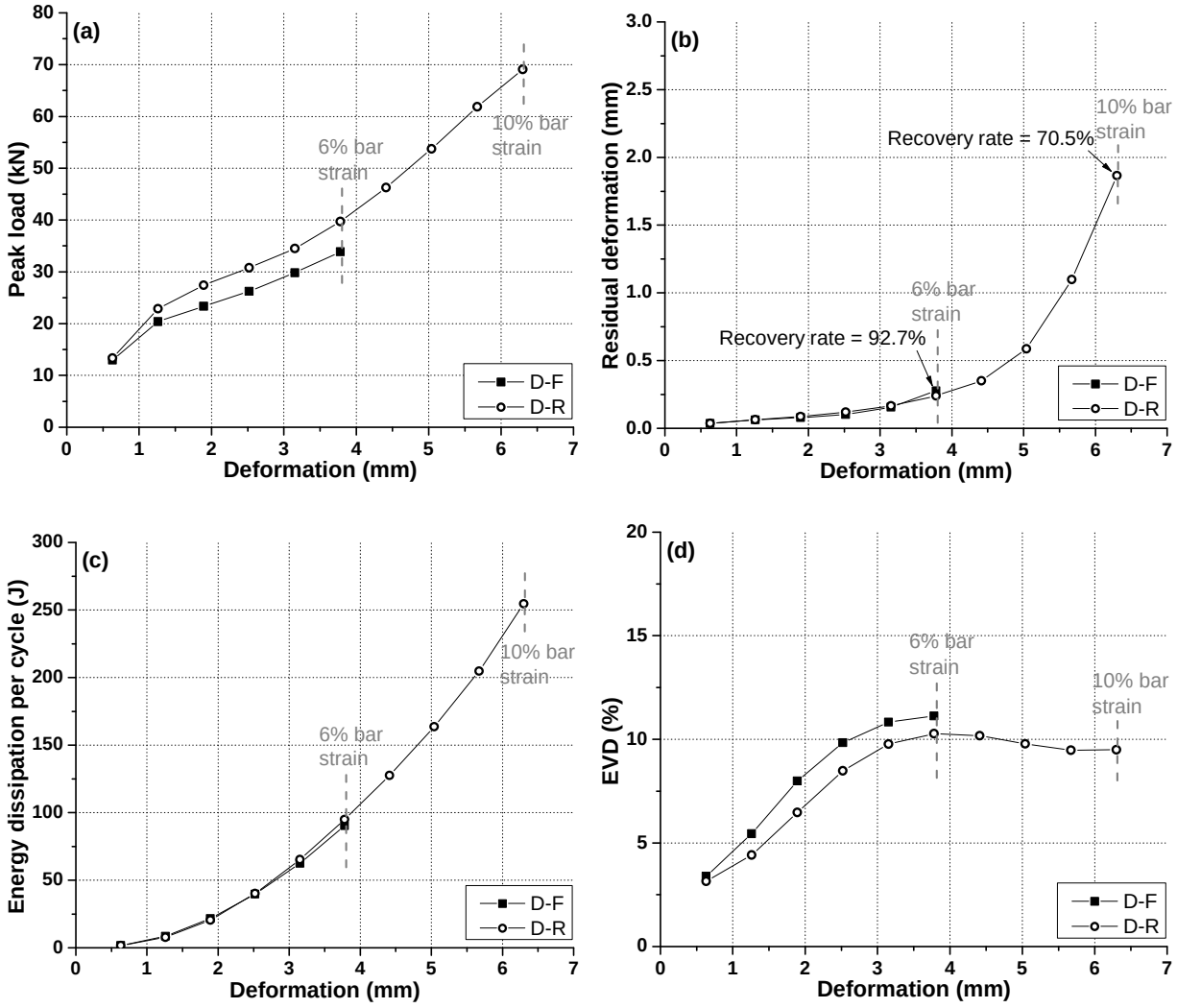

Fig. 8 Cyclic performances of damper specimens: a) peak load, b) residual deformation, c) energy dissipation per cycle, d) EVD

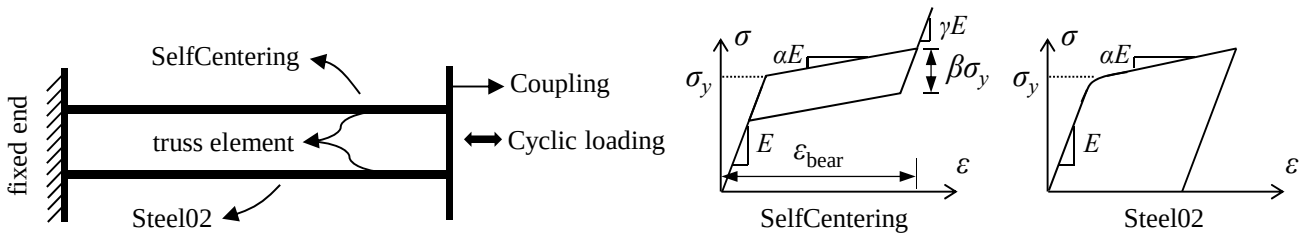

(a)

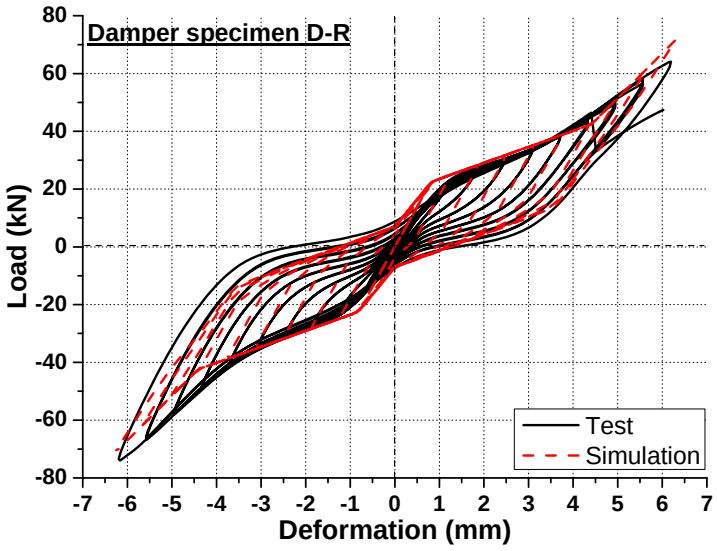

(b)

Fig. 9 Modelling of damper in OpenSees: (a) illustration of FE model, (b) simulation result

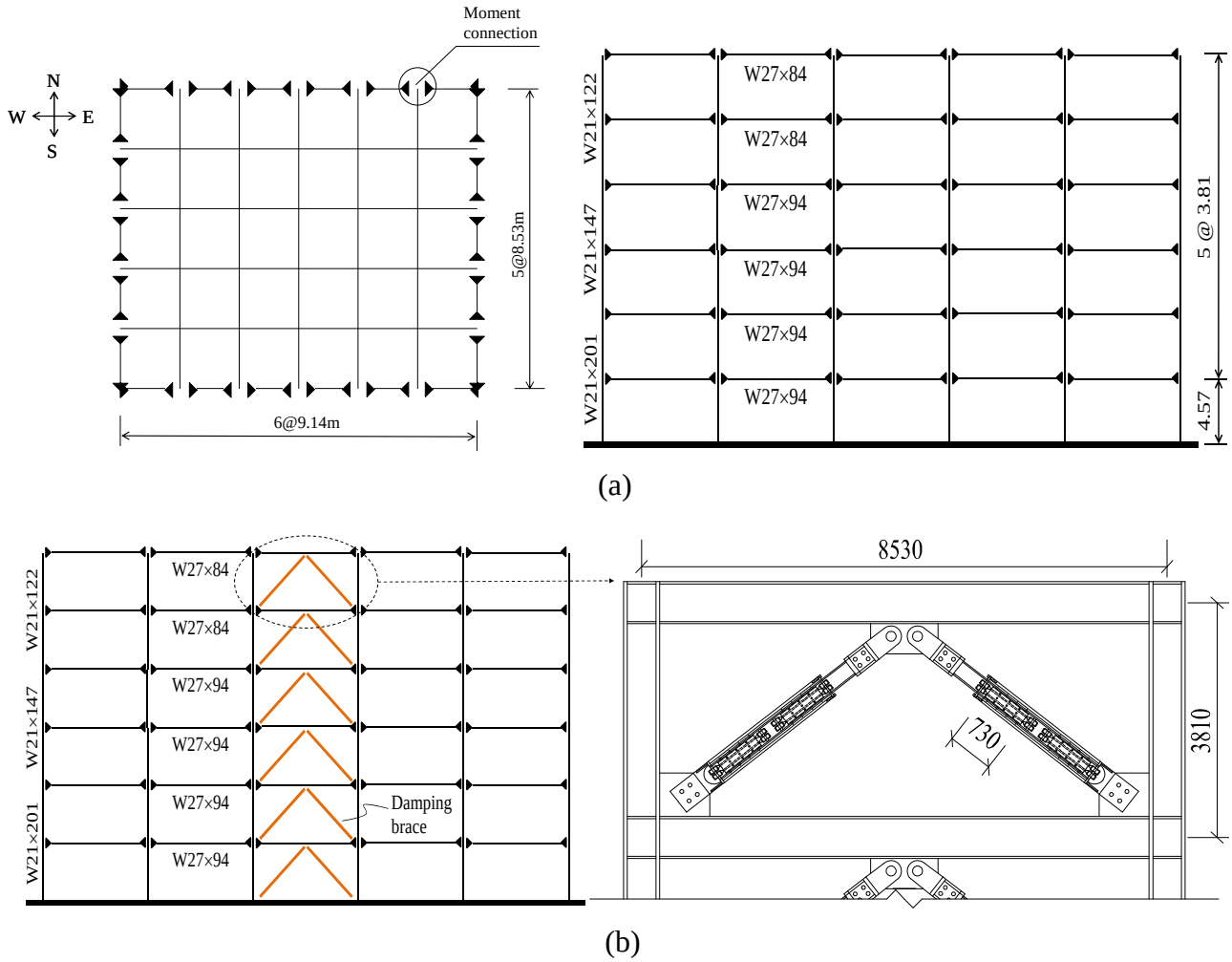

Fig. 10 Considered frame buildings: (a) plain layout and elevation view of original prototype frame, (b) retrofitted braced frame

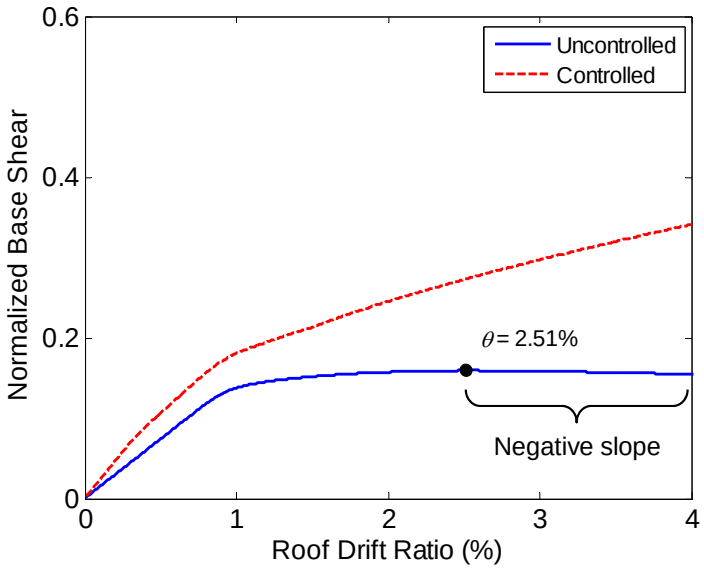

Fig. 11 Static pushover responses of uncontrolled and controlled frames

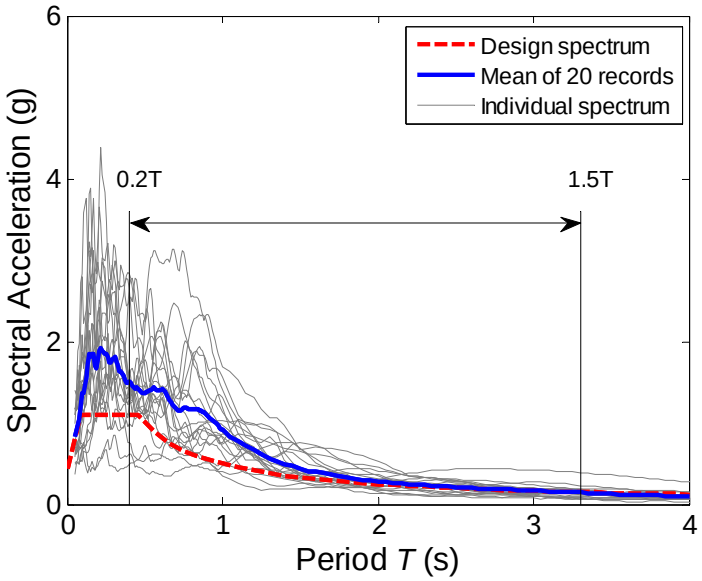

Fig. 12 Response spectra of ground motion records

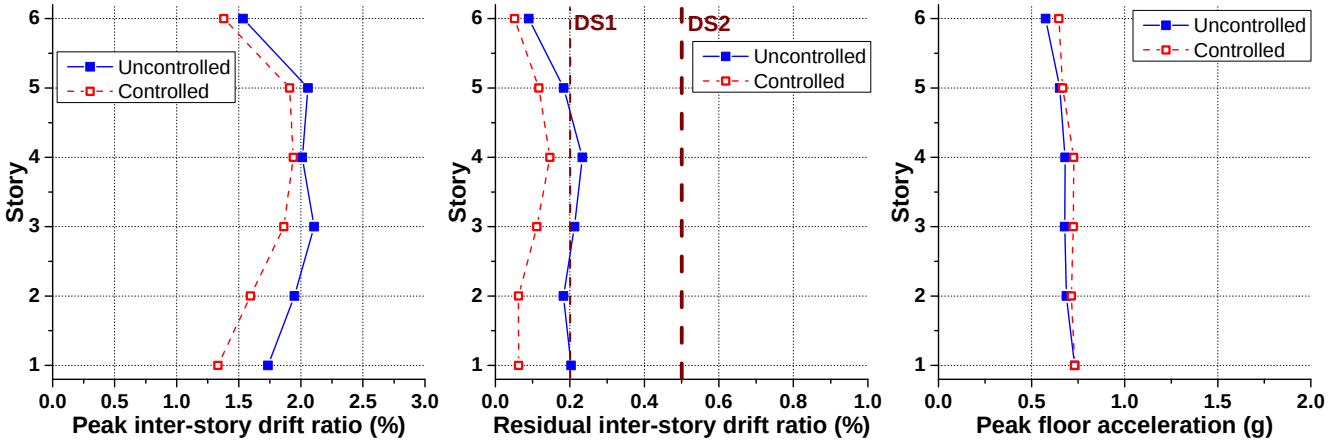

(a)

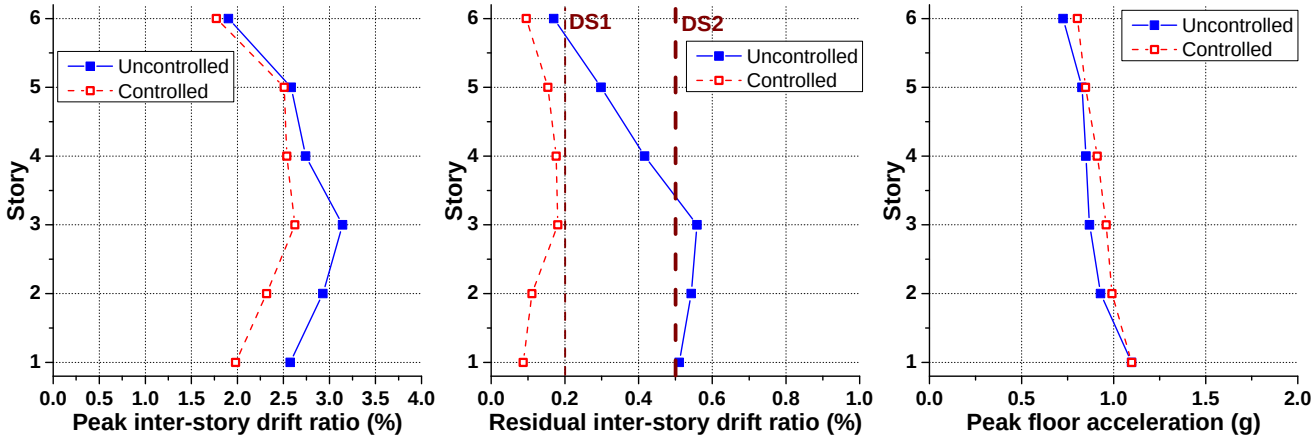

(b)

Fig. 13 Comparisons of structural responses between uncontrolled and controlled frames: (a) DBE responses, (b) MCE responses

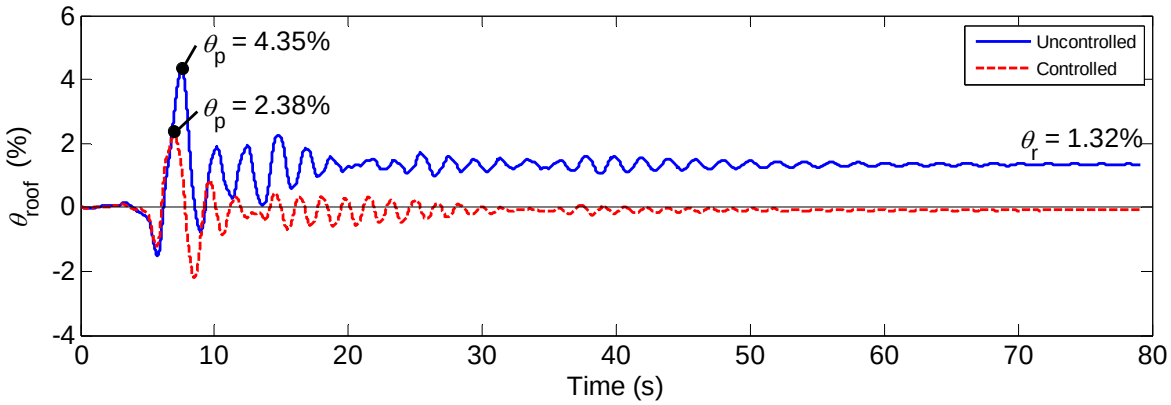

(a)

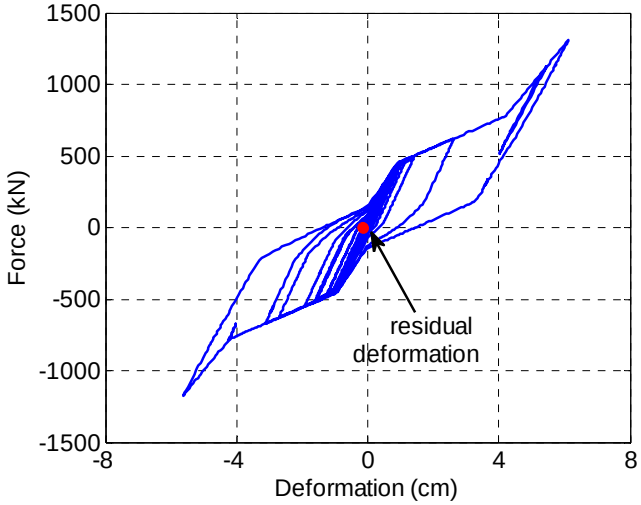

(a)

Fig. 14 Typical behavior of uncontrolled and controlled frames under ground motion SE01 × 1.5: (a) roof drift time-history response, (b) cyclic behavior of 4th-story SMA damper

Table 1 Testing parameters for individual bars

Test code	Section type	Working length (mm)	Cross-sectional area (mm^2)
SMA-R-1	Round	63	28.27
SMA-R-2	Round	63	56.75
SMA-F-1	Flat	63	28.61
SMA-F-2	Flat	63	56.02
Steel	Round	118	113.04

Table 2 Fundamental material properties of SMA bars

Test code	Young's modulus (GPa) +/-	"Yield" strength (MPa) +/-	EVD* +/-
SMA-R-1	32.2/40.9	377.6/468.0	5.9%/5.3%
SMA-R-2	36.0/38.6	378.8/503.0	4.4%/6.0%
SMA-F-1	40.8/42.6	456.3/367.9	5.3%/6.3%
SMA-F-2	36.8/38.5	371.3/376.8	5.5%/6.4%

Note 1: * is based on the average value at 5% strain
Note 2: +/- mean tension and compression behavior, respectively

Table 3 Input parameters for damper model

Material	A (mm^2)	L (mm)	σ_y (MPa)	E (GPa)	α	β	ε_{bear}	γ
SelfCentering	33.9	63	400	31	0.17	1.0	0.06	0.8
Steel02	22.6				0.25	-	-	-

Table 4 Properties of SMA damping braces in controlled frames

Story No.	"Yield" strength (kN)	Initial stiffness (kN/mm)	SMA bars		
			Diameter (mm)	Pairs of SMA bars	Effective length (m)
1	949.9	93.2	27	2	0.81
2	791.6	86.8	25	2	0.73
3	497.6	54.5	20	2	0.73
4	452.3	49.6	19	2	0.73
5	361.9	39.7	17	2	0.73
6	316.6	34.7	16	2	0.73